Tectonophysics 700–701 (2017) 19–31

Contents lists available at ScienceDirect

Tectonophysics

journal homepage: www.elsevier.com/locate/tecto

Detection of a new sub-lithospheric discontinuity in Central Europe with S-receiver functions

Rainer Kind [a,b,*], Mark R. Handy [b], Xiaohui Yuan [a], Thomas Meier [c], Horst Kämpf [a], Riaz Soomro [d]

[a] GFZ German Research Center for Geosciences, Telegrafenberg, 14473 Potsdam, Germany
[b] Freie Universität, Institut für Geologische Wissenschaften, Malteserstrasse 74-100, 12249 Berlin, Germany
[c] Christian-Albrechts Universität, Institut für Geowissenschaften, Otto-Hahn-Platz 1, 24118 Kiel, Germany
[d] Seismic Studies Programme, Nilore, Islamabad 44000, Pakistan

ARTICLE INFO

Article history:
Received 10 September 2016
Received in revised form 30 January 2017
Accepted 6 February 2017
Available online 13 February 2017

Keywords:
Lithosphere-asthenosphere boundary (LAB)
Mid-lithospheric discontinuity (MLD)
Sub-lithospheric discontinuity (SLD)
S-receiver functions
East European Craton
Bohemian Massif
Pannonian Basin

ABSTRACT

We used S-receiver functions (i.e. S-to-P converted signals) to study seismic discontinuities in the upper mantle between the Moho and the 410 km discontinuity beneath central Europe. This was done by using c. 49,000 S-receiver functions from c. 700 permanent and temporary broadband stations made available by the open EIDA Archives. Below Phanerozoic Europe we observed expected discontinuities like the Moho, the lithosphere-asthenosphere boundary (LAB), the Lehmann discontinuity and the 410 km discontinuity with an additional overlying low velocity zone. Below the East European Craton (EEC), we observed the Mid-Lithospheric Discontinuity (MLD) at c. 100 km depth as well as the controversial cratonic LAB at c. 200 km depth. At the boundary of the EEC but still below the Phanerozoic surface, we observed downward velocity reductions below the LAB in the following regions: the North German-Polish Plain at about 200 km depth; the Bohemian Massive, north-west dipping from 200 to 300 km depth; the Pannonian Basin, north-east dipping from 150 to 200 km depth underneath the western Carpathians and the EEC. We named this newly observed structure Sub-Lithospheric Discontinuity (SLD). At the northern edge of the Bohemian Massive, we see a sharp vertical step of about 100 km between the SLD below the Bohemian Massive and the North German-Polish Plain. This step follows the surface trace of the Rheic Suture between the continental Saxo-Thuringian and Rheno-Herzynian zones of the Variscan orogen. A preliminary interpretation of these features is that a prong of the cratonic mantle lithosphere penetrated the Phanerozoic asthenosphere during the continental collision at the western and south-western edges of the EEC.

1. Introduction

The basic geology of central Europe north of the Alps is highly complex and determined by the Caledonian and Variscan orogenies which resulted from the collision of the plates of Gondwana and Laurussia, and numerous Peri-Gondwanan related microterranes which lay in between. Especially the closing of the Rheic Ocean in the Paleozoic (e.g. Linnemann, 2007; Nance and Linnemann, 2008; Zeh and Gerdes, 2010; Kroner and Romer, 2013) caused subduction, volcanisms and accretion of a number of terrains (e.g. Bohemian Massif or Rhenish Massif). The geology of the Mediterranean area is determined by the Alpine orogeny which is caused by the collision of the African plate with the European plate and several microplates (Adria, Iberia, Anatolia) since the late Mesozoic (e.g. Faccenna et al., 2014). The Alps, the Apennines, the Dinarides and Carpathians are expressions of this collision (see Fig. 1 for location of tectonic boundaries). The Tornquist-Teisseyre Zone (TTZ) is the most significant structure in Europe which separates the East European Craton (EEC) from Phanerozoic Europe. Finding the cause of this dynamics of the lithospheric plates requires integrating images of deep structures with surface geology which preserves the records of motion back in time. Here we are studying the deep structure. There are numerous seismic techniques used for studying discontinuities in the upper mantle. The oldest technique is wide angle seismics where the horizontal ray path is much longer than the vertical one. Gutenberg (1926) found with this technique the downward velocity reduction in the oceanic upper mantle at 60–80 km depth which bears his name. He concluded that the mantle was crystalized to that depth. There are many wide and steep angle controlled source profiles which sample the structure of the continental mantle below the Moho in northern Europe, North America and other regions. North of the Alps and beneath Paleozoic Europe, the Moho is relatively flat at a depth of about 30 km and shows no significant lateral variations (Grad et al., 2009). Geology indicates a complex history of accretion and subduction, followed by late- to post-Variscan magmatism and oblique-slip tectonics (e.g., Matte, 1998; Franke, 2000, 2014). Accordingly, the overall laterally continuity of the European Moho is attributed to this post-Variscan

* Corresponding author at: GFZ German Research Center for Geosciences, Telegrafenberg, 14473 Potsdam, Germany.
E-mail addresses: kind@gfz-potsdam.de (R. Kind), mark.handy@fu-berlin.de (M.R. Handy), yuan@gfz-potsdam.de (X. Yuan), meier@geophysik.uni-kiel.de (T. Meier), kaempf@gfz-potsdam.de (H. Kämpf), riaz_soomro@yahoo.com (R. Soomro).

http://dx.doi.org/10.1016/j.tecto.2017.02.002
0040-1951/

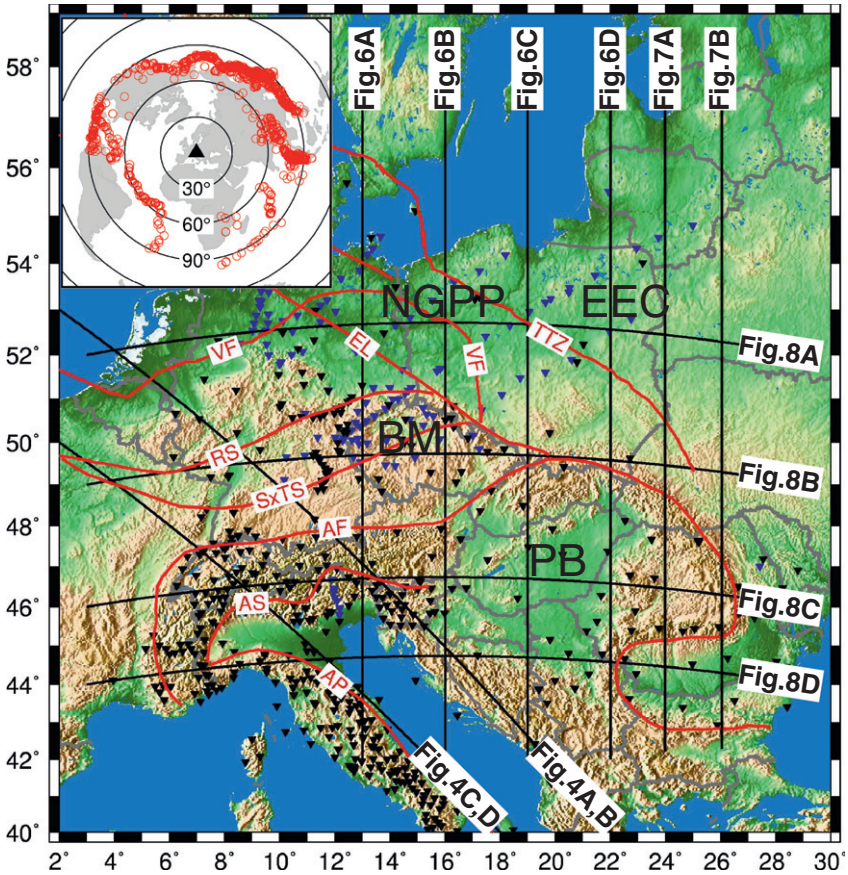

Fig. 1. Map of seismic broadband stations used in this study. Black: permanent stations, blue: temporary stations. Major tectonic boundaries marked in red: TTZ - Tornquist-Teisseyre Zone, VF - Variscan Front, EL - Elbe Line, RS - Rheic Suture, SxTS - Saxo-Thuringian Suture, AF -Alpine Front, AS - Alpine Suture, AP - Apenninic Front, Dinaric Front. Tectonic units: PB - Pannonian Basin, EEC - East European Craton, NGPP - North German-Polish Plain, BM - Bohemian Massif. Upper lefthand corner - epicenters of earthquakes used in this study.

thermal and magmatic equilibration (Oncken, 1998). In contrast, in Proterozoic and Archean cratons many inclined structures below the Moho have been observed and interpreted as remnants of subduction zones (e.g., Babel Working Group, 1990; see also Steer et al., 1998 for a summary). Bostock (1998) confirmed in the Slave craton in Canada the existence of such structures with receiver function data down to about 200 km depth. Balling (2000) interpreted in controlled source data north-dipping structures in the Baltic sea and south-dipping structures in the North Sea as remnants of fossil subduction zones. Thybo and Perchuc (1997) concluded mainly from wide angle controlled data the global existence of a low velocity zone in cratons near 100 km depth (the 8° discontinuity). At lower crustal depths the location of the tectonic boundaries in northern central Europe is under discussion (see e.g. Rabbel et al., 1995). Likely it is of Avalonian origin but altered by post-Caledonian processes. Gossler et al. (1999) and Bayer et al. (2002) concluded that the lower crust of the East European Craton extends to the Elbe Line below the Caledonian upper crust. Steep angle reflection projects in Germany (DEKORP) found only isolated events of inclined structures below the Moho which have been interpreted as remnants of fossil subduction (e.g. Meissner and Rabbel, 1999).

Seismic tomography is probably the most-used method to study velocity anomalies in the upper mantle. Gradual velocity changes are resolved by this technique but it is less sensitive to seismic discontinuities (velocity jumps of c. 5–10% over c. 0–30 km depth range). Several groups have produced tomographic images of the European and Mediterranean area (Zielhuis and Nolet, 1994; Marquering and Snieder, 1996; Villaseñor et al., 2001; Koulakov et al., 2009; Bijwaard and Spakman, 2000; Legendre et al., 2012; Zhu et al., 2012, 2015; Zhu and Tromp, 2013; Auer et al., 2014; Meier et al., 2016). The results show that under the East European Craton the velocities, in particular the shear-wave velocity, increase in the mantle lithosphere by up to 6%. According to these studies, the cratonic mantle lithosphere is about 250 km to 300 km thick. In contrast, shear-wave velocities are low in the upper mantle beneath central Europe and the Pannonian Basin and the thickness of the lithosphere decreases locally to about 50 km to 60 km. Intermediate lithospheric thickness is observed between the Tornquist–Teisseyre Zone and the Elbe Line (e.g., Legendre et al., 2012).

P-wave tomographic studies of the Alps (Lippitsch et al., 2003; Mitterbauer et al., 2011) and of the greater Alpine region (Piromallo and Morelli, 2003; Spakman and Wortel, 2004; Giacomuzzi et al., 2011) indicate a south-east dipping anomaly beneath the central Alps, interpreted as subducted European lithosphere. More detailed studies of the area suggest along-strike changes in slab orientation beneath the Central and Eastern Alps. Lippitsch et al. (2003) interpreted a subvertical to NNE-dipping anomaly as Adriatic lithosphere (Schmid et al., 2004) which has since been supported by additional tomography (Karousova et al., 2013). Other studies conducted at somewhat lower resolution (Spakman and Wortel, 2004; Mitterbauer et al., 2011) show ambiguous polarity, with the latter authors arguing for a continuous European slab beneath the Alps which becomes subvertical to steeply N-dipping beneath the eastern Alps. P-wave tomography models indicate a slab gap below the northern Dinarides (Bijwaard and Spakman, 2000; Piromallo and Morelli, 2003; Spakman and Wortel,

2004; Koulakov et al., 2009; Serretti and Morelli, 2011; Legendre et al., 2012; Zhu et al., 2012, 2015). However, Sumanovac and Dudjak (2016) do not see a gap but a continuous slab in the northern Dinarides.

A more recent technique is the receiver function method which is sensitive to seismic discontinuities, but less to gradual velocity changes (e.g., Kind et al., 2012). The discontinuities usually observed in the upper mantle with receiver functions are the crust-mantle boundary (Moho), the lithosphere-asthenosphere boundary (LAB), a relatively recently found Mid-Lithospheric Discontinuity (MLD, Yuan and Romanowicz, 2010) beneath cratons, the discontinuities bordering the upper mantle transition zone at 410 and 660 km depth, occasionally the Lehmann discontinuity (Lehmann, 1959) and perhaps other additional discontinuities (see for the central and northern European areas: Gossler et al., 1999—Moho in northern Germany, Denmark and Sweden; Alinaghi et al., 2003—Moho, 410 and 660 in northern Germany, Denmark, Sweden and Finland; Kummerow et al., 2004—Moho, 410 and 660 below the eastern Alps; Wilde-Piorko et al., 2010—Moho, LAB, 410 and 660 across the TTZ; Heuer et al., 2006, 2007, 2011—Moho, LAB, 410 and 660 below Bohemia; Sodoudi et al., 2006, 2015—Moho and LAB below the Aegean; Geissler et al., 2008, 2010, 2012—Moho, LAB, 410 and 660 below Bohemia, Europe; Lombardi et al., 2008, 2009—Moho, 410 and 660 below the Alps; Jones et al., 2010—LAB in Europe; Hrubcova and Geissler, 2009—Moho below Bohemia; Plomerova and Babuska, 2010—LAB in Europe; Miller and Piana Agostinetti, 2012—Moho and LAB below Italy; Knapmeyer-Endrun et al., 2013, 2017—LAB, MLD, 410 and 660 across the TTZ; Bianchi et al., 2014—Moho and LAB below the eastern Alps). In receiver function processing we usually assume the discontinuities are horizontal. Strongly inclined discontinuities generate less converted waves. Schneider et al. (2013) and Kind et al. (2015b) discussed P-receiver functions generated at inclined discontinuities and found that good results are obtained for inclinations up to about 30°. S-receiver functions at inclined subduction zones are commonly observed (e.g., Sodoudi et al., 2011). However, it should be mentioned that waves converted in the heterogeneous Earth are scattered waves and they are sensitive to any kind of sharp local heterogeneity.

The LAB and MLD of the EEC are so far not very well imaged with the exception of the neighboring Scandinavia where more data are available (Kind et al., 2013) and very recently across the TTZ (Knapmeyer-Endrun et al., 2017). The question if the LAB of cratons is observed in receiver functions is a far reaching problem because it is an indication of the sharpness of this discontinuity. Such observations would indicate that the cratonic LAB could not be caused by temperature changes alone (see e.g., Kind et al., 2015a; Hopper and Fischer, 2015). Another still open question in craton formation is the nature of the MLD. There are several suggested explanations (Mierdel et al., 2007; Karato et al., 2015; Selway et al., 2015; Rader et al., 2015). Hopper and Fischer (2015) discussed these suggested solutions. Their preferred model of the MLD is a layer of frozen-in volatile-rich melt. The shear velocity reduction may be caused by the presence of phlogopite or amphibole. Rader et al. (2015) conclude that the MLD could be interpreted as a remnant of the LAB of the emerging craton. Seismic observations may support this view, since receiver function signals from the LAB of tectonically active margins of cratons are undistinguishable from the MLD signals within cratons (e.g., Kind et al., 2013; Knapmeyer-Endrun et al., 2017). Our intention at present is to use the largely untapped data base of teleseismic S waves in the European open data archives to derive higher resolution S receiver functions and thus to contribute to the detection of upper mantle discontinuities and their topography beneath the North German-Polish Plain (NGPP), the Bohemian Massif (BM), the Alps, the Pannonian Basin (PB) and the SW part of the East European Craton (EEC).

2. Data and data processing

The seismic data used in this study are recorded by about 580 permanent and 120 temporary broadband stations in Europe. A disadvantage of the permanent station is their sparse distribution in some regions. However, it is an advantage of S-receiver functions that they sample much larger regions than P-receiver functions. Therefore most regions are sampled with data from several stations recording events from different epicentral distances and backazimuths. The data are archived in several data centers (e.g., ORFEUS in Utrecht (orfeus-eu.org), GEOFON in Potsdam (gfz-potsdam.de/geofon) or the INGV in Rome (ingv.it)) and made freely available to any user. The data are accessed via the EIDA portal (European Integrated Data Archive, e.g., eida.gfz-potsdam.de) which makes the access to all centers very convenient. We obtained data from about 1500 earthquakes. The number of earthquakes recorded by each station is very different. There are only 80 stations which have more than a hundred useful records. A map of the seismic stations and epicenters of earthquakes used is shown in Fig. 1. We have checked all data visually and selected events with a signal-to-noise ratio of at least two of the S signal on the Q component. We also did not use events with high noise level before the S signal on the L component or with poor approximation of the delta function on the Q component after deconvolution. The last step seems to be important since there has been a relatively large number of traces with poor deconvolution. The receiver function method is described in many papers (e.g., Kind et al., 2012). The rotation from the original *Z*-N-E coordinate system into the ray L-Q-T system was done with theoretical backazimuth and incident angles. We used wave shaping time domain deconvolution. Our selection criteria seem very robust since different people working with the data, including students, arrived at very similar results. In total we have obtained about 49,000 useful S-receiver functions. Fig. 2 shows a map of all the S-to-P piercing points at 200 km depth. Regions with highest piercing point density are the ones with highest reliability of the observational results. The diameter of the Fresnel zone is about 130 km at 200 km depth assuming a period of 8 s.

The data have been band-pass filtered between 8 and 50 s. Unfiltered data would lead to more scattered images (Fig. 3). Comparing the unfiltered shorter period data in Fig. 3A with the longer period data (bandpass 8–50 s) in Fig. 3B we note that the Moho, the 410 km discontinuity and the LVZ above the 410 have also shorter period signals in Fig. 3A than in Fig. 3B. This indicates that these discontinuities are indeed single and sharp discontinuities. However, the LAB and the SLD appear in the short period data (Fig. 3A) not as single discontinuities but are split into several more heterogeneous discontinuities scattered over a depth range of about 10 km. This means that in contrast to the Moho, the 410 and the LVZ the LAB and SLD consist of several relatively sharper discontinuities scattered over a depth range of about 10 km. Similar observations have been made for the upper mantle discontinuities in North America (Kind et al., 2015a).

The final steps in the data processing were the migration from the time domain into the depth domain (Dueker and Sheehan, 1997; Jones and Phinney, 1998; Kosarev et al., 1999) along the ray path of the S phase within the IASP91 global reference model (Kennett and Engdahl, 1991) and spatial smoothing of the data.

We have assembled the migrated data along depth profiles. In Fig. 4A and B are shown effects of different profile widths on the data image. We used lateral profile widths between 200 and 400 km. Such large widths were required to obtain a high signal-to-noise ratio of the conversions since the spacing between the permanent stations is relatively large. We cannot give a general minimum number of required traces for summation, since this number varies strongly with local conditions. Fig. 4A and B show that 400 km profile width produces clearly a better signal-to-noise ratio, although in the 200 km profile wide profile the significant signals can be identified too. For the migration we divided the Earth model into 3 × 3 km boxes in vertical and in profile direction. This

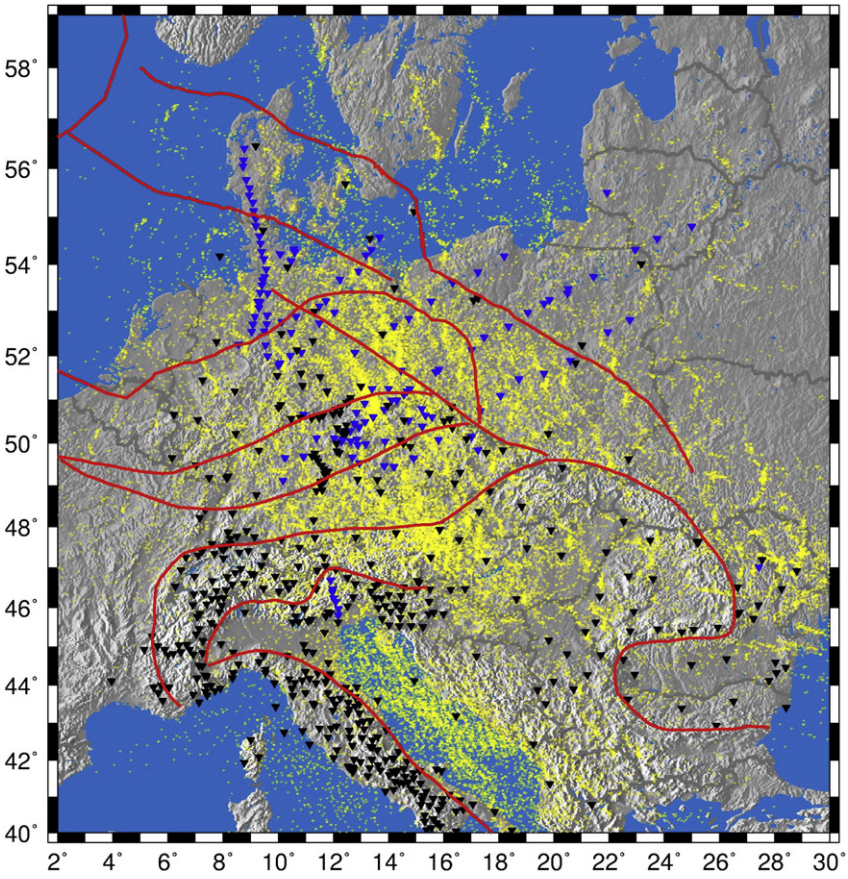

Fig. 2. Piercing point distribution (yellow dots) at 200 km depth of all seismograms used. Regions with piercing point concentrations have the most reliable information.

is oversampled for the wavelengths we used (~8 s period, ~40 km wavelength) but it leads to smoother images and the computation time is still no problem. For the smoothing along the profile and in vertical direction we used the GMT (Generic Mapping Tools, Wessel and Smith, 1998) within 3 km vertical and 150 km horizontal smoothing interval (which corresponds to the size of the Fresnel

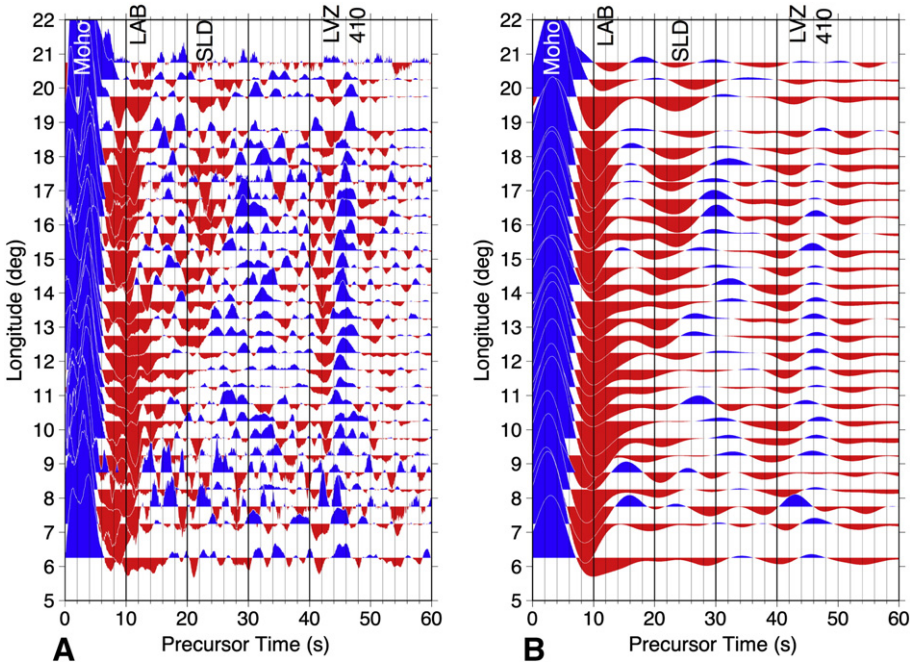

Fig. 3. East-west S-receiver function profile between Bohemian Massif and Baltic Sea in time domain. A - no filter applied, B - 8–50 s band-pass filter applied. All marked phases are clearly visible in B, whereas in the unfiltered data in A only the Moho, LVZ and the 410 remain as relatively sharp discontinuities. The LAB and SLD appear as broad scattered signals. This may indicate that there is a fundamental difference in discontinuity structure between the LAB and SLD relative to the other discontinuities.

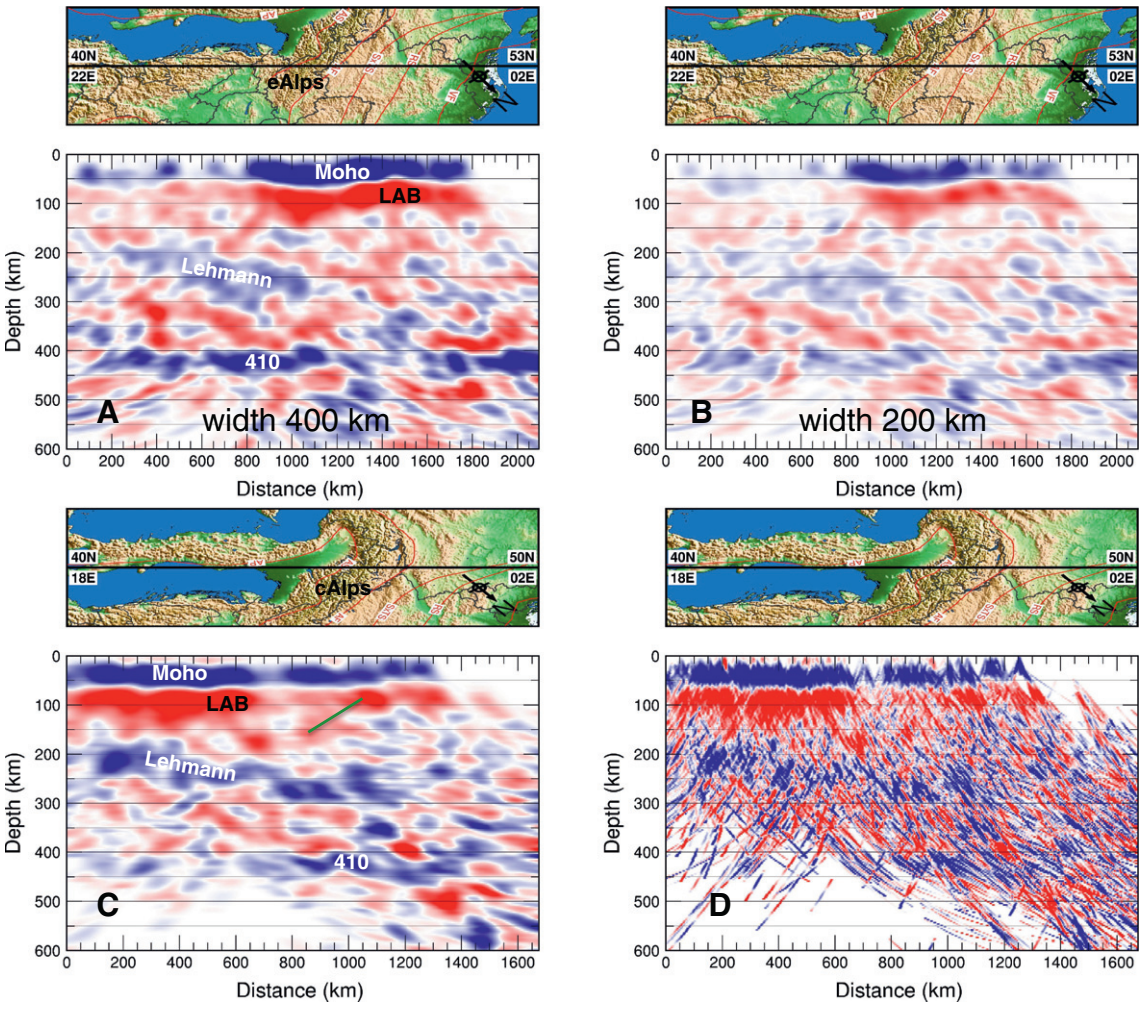

Fig. 4. (A) and (B): Comparison of migrated S-receiver function profiles with different widths: (A) 400 km and (B) 200 km. (C) and (D): Comparison of different smoothing intervals used in the GMT routines. (C) 3 km vertical times 150 km horizontal and (D) 3 km vertical times 3 km horizontal. The green line in C marks the possible LAB of the European slab below the central Alps. See Fig. 6 for explanation of seismic signals. The eastern and central Alps are marked in the maps with eAlps and cAlps. See Fig.1 for location of tectonic units and profiles.

zone) and cosine arch weighting (Fig. 4A and B). We illustrate in Fig. 4C and D the effects of different smoothing parameters.

3. Computation of theoretical seismograms and comparison with observed data

In this section we compare upper mantle structures obtained from surface wave tomography with those obtained from S-receiver functions. We use a tomography model, compute the theoretical seismograms and compare with the observed S-receiver functions. Surface waves are sensitive to shear-wave velocities down to about 300 km depth. One-dimensional models of absolute shear-wave velocity (see Fig. 5D) in central Europe are obtained by inversion of local dispersion curves, which are determined by surface wave tomography (Soomro et al., 2016; Meier et al., 2016). An iterative gradient search inversion following Meier et al. (2004) is applied. Velocities in the crust as well as the Moho depth are strongly damped towards the background models derived from the crustal model EuCRUST-07 (Tesauro et al., 2008). Below the Moho the background models follow the global ak135 model (Kennett et al., 1995). Note that because of possible trade-offs between shear-wave velocities above and below the Moho and the Moho depth, unrealistic estimates of the shear-wave velocity obtained from the crustal background model may propagate into uncertain velocities in the uppermost mantle directly below the Moho.

Enlarged shear-wave velocities in the upper mantle for the model for the EEC (blue model in Fig. 5D) indicate the cratonic mantle lithosphere of the EEC. In contrast, the red model for central Europe shows the presence of a shallow asthenosphere and the green model shows a lithospheric thickness of about 120 km for the region of the North German Basin. Due to the smooth nature of the surface wave sensitivity kernels, the depth of the LAB is more difficult to estimate from inversion results of surface waves but can be approximately found in the middle of the gradient zone between lithospheric mantle and asthenosphere (e.g., Bartzsch et al., 2011).

In the following we compute theoretical seismograms of these models to see what signals could be expected in S-receiver function data. We used the version of the reflectivity method by Kind (1985) which has different crustal models at the source and receiver sides and no multiples like PP are included. We also used the IASP91 global model with the source side crust omitted in order to avoid its influence on the seismograms. The theoretical radial and vertical component seismograms are rotated in L and Q components. No deconvolution was applied since the source signal is simple and the source side structure is not influencing this signal. S-to-P conversions at the Moho and the 410 km discontinuity (blue) are clearly observed in Fig. 5A, B and C. The negative gradient in the red model in D (Central European Platform) produces in A the red negative signal (marked by the red arrow). As explained above the complicated structure in the green

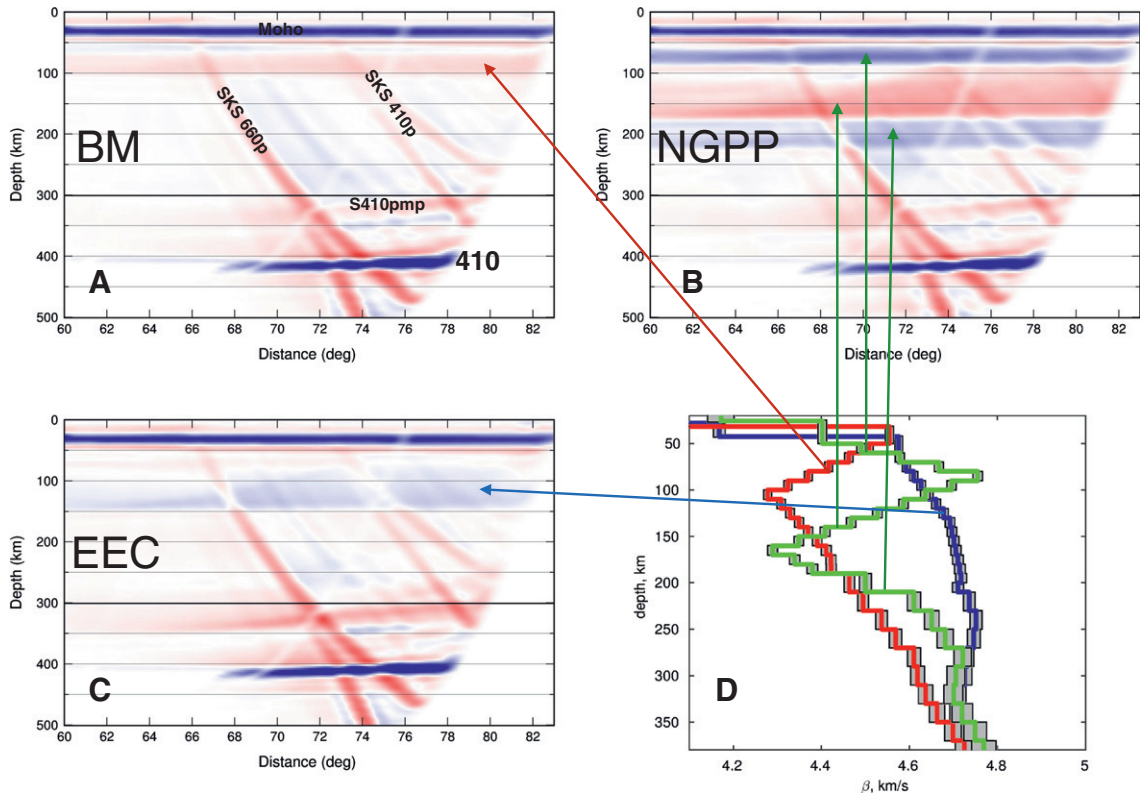

Fig. 5. A, B, C - Theoretical seismograms for the receiver side upper mantle shear velocity models in D, which are derived from surface wave tomography (Soomro et al., 2016). Plotted is the depth migrated L-component as function of the epicentral distance. The main period of the input signal is 6 s. A: red model in D, Bohemian Massif (central Europe); B: green model in D, North German-Polish Basin; C: blue model in D, East European Craton. The signals marked "S410pmp" are P multiples within the crust below the stations of the S wave converted to P at the 410 km discontinuity. Arrows indicate connections between seismic signals and causal parts of the model. The SKS410(660)p signals will be erased after common station or common conversion point summation of many traces from many different epicentral distances since their slowness differs significantly from the slowness of the conversions of the S phase.

model (North German Basin) between 50 km and 100 km is likely due to deviations of the crustal background model from the real structure resulting in several signals at those depths. This model produces several signals in the theoretical receiver functions in B: a positive (blue) signal between 50 and 100 km depth; a negative signal (red) between 100 and 170 km depth; and another positive signal (blue) near 200 km depth. The main period of the theoretical seismograms is about 6 s corresponding to about 50 km wave length. Interestingly, the gradients in the 1D models obtained by inversion of surface wave dispersion curves are strong enough to give rise to S-P converted phases. The signals marked "Moho multiples" in Fig. 5A and also visible in Fig. 5B and C are P multiples in the crust below the stations. It is usually said that S-receiver functions do not produce multiples before S. This, however, means only that crustal multiples of the S signals do not arrive before S. However, P crustal multiples of P waves below a station caused by S-to-P conversions at upper mantle discontinuities (S410pmp) may still arrive before the S signal and need possibly to be taken into account, although they have not been observed in data so far.

The theoretical S-receiver functions of surface wave tomography models in Fig. 5A agree qualitatively well with our observed S-receiver functions in Fig. 4A and B for approximately the same region. A velocity reduction is observed with both techniques at about 50–100 km depth. This is encouraging for a later quantitative comparison of both techniques. The theoretical S-receiver functions of the tomography model of the North German-Polish Plate (Fig. 5B) do not agree as well with the observations of the flat part of the SLD structure in Fig. 6A and B in about the same region. In the theoretical S-receiver functions we see two positive structures (blue) whereas we see two negative structures in the observed data. Although results of both methods do not agree very well, at least they indicate a layered structure in this region. Comparing theoretical S-receiver functions of the East European Craton (Fig. 5C) with the data in Fig. 6, we see that the data have a negative structure near 200 km depth, whereas the computations show a positive structure at 100–150 km depth. The reason why tomography and receiver function results disagree in some cases are difficult to evaluate. We should recall the principal differences of both techniques: tomography is insensitive to discontinuities, receiver function are insensitive to gradual changes. It should be mentioned that we did not find evidence for crustal multiples in our data which are caused by the theoretical S410p phase shown in the theoretical seismograms in Fig. 5.

4. Profiles across the European mantle

We have produced two suites of east-west and north-south profiles across the European mantle which are shown in their entirety in Supplementary material (Figs. S1 and S2). Here we show only several informative examples.

In Fig. 6 are shown four north-south profiles. The two profiles in Fig. 6A and B range from eastern Alps (marked eAlps) across the Bohemian Massif to the North German-Polish Plain entirely through Phanerozoic area. They show a number of seismic phases which can be correlated over hundreds of kilometers. We see the well-known Moho and the discontinuity at 410 km depth at their expected locations. We should mention here that the depth of a discontinuity is measured at the center of the blue or red signal due to the deconvolution used in the processing. The Moho and the 410 km discontinuities are not the goal of our study. They serve here merely as indication of the reliability of the data. We are trying to identify additional major phases which are coherent over larger distances and broader regions.

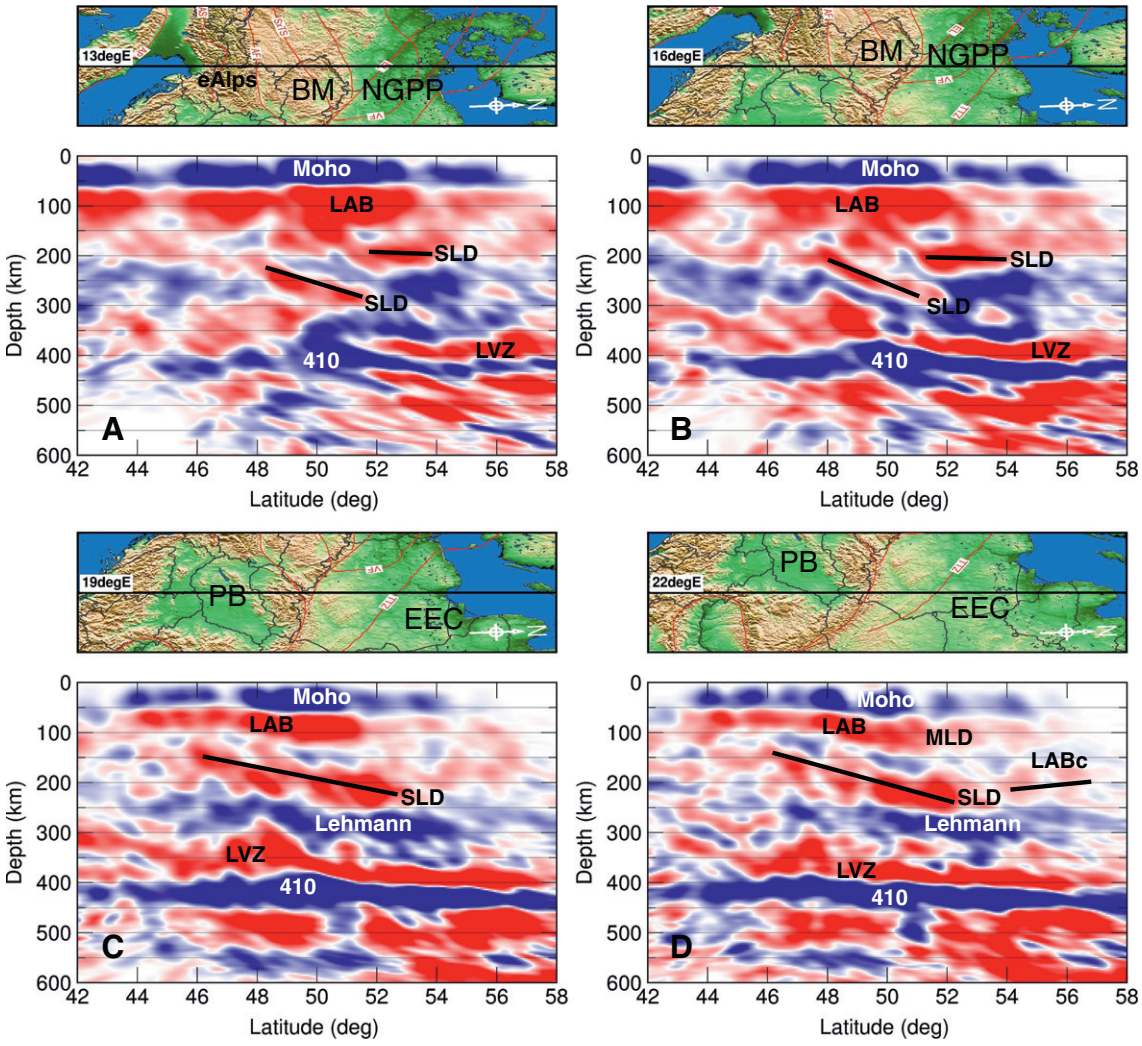

Fig. 6. Four north-south S-receiver function profiles at 13°E (A), 16°E (B), 19°E (C) and 22°E (D). The width of the profiles is 400 km, i.e., 200 km on either side of the black profile line in the top panels. Blue colors mark seismic discontinuities with velocity increasing downward, red colors indicate velocity reducing downward. Additional north-south profiles are displayed in Fig. S2, Supplementary material. Abbreviations: Moho - crust-mantle boundary, LAB - Phanerozoic Lithosphere-Asthenosphere Boundary, MLD - Mid-Lithospheric Discontinuity in the EEC, LABc - cratonic LAB in the EEC, Lehmann - Lehmann discontinuity (frequently interpreted as bottom of the asthenosphere), LVZ - top of low-velocity zone above the 410 km discontinuity, 410–410 km discontinuity. The newly observed negative discontinuity below the LAB is marked SLD. The Lehmann discontinuity is not marked in Fig. 6A and B because it is very scattered there and it is unknown if this is real or perhaps due to insufficient data (compare Figs. 19 and 20 in Fig. S2 Supplement). The lack of lateral continuity of the 410 in A is probably caused by laterally inhomogeneous data coverage.

The known subduction of the European lithosphere below the central Alps is visible in north-south profiles in Fig. S2, slides 3–8 of the Supplementary material. In the four profiles in Fig. 6 we have marked an additional signal SLD. This signal is visible at the two eastern profiles in Fig. 6C and D a continuous signal dipping from 150 km depth below the Pannonian Basin and continuing underneath the western Carpathians to about 250 km below the East European Craton. In Fig. 7 is shown the possible connection of the SLD with the cratonic LAB (marked LABc in Fig. 7) in four north-south profile across the boundary of the East European Craton and Phanerozoic Europe. The depth of the LABc is near 200 km in good agreement with the expected depths. Similar signals from the bottom of the cratonic lithosphere are observed in North America and in Scandinavia (Kind et al., 2013, 2015a). Knapmeyer-Endrun et al. (2017) also observed the MLD east of the TTZ along with weak indications of the cratonic LAB, but no indication of the SLD west of the TTZ.

It should be noted that below the Pannonian Basin the Phanerozoic LAB is observed at a relatively shallow depth of about 70–80 km and deepens towards the East European Craton where it is marked MLD (Fig. 6D). We notice that there is no difference in the appearance of the seismic signals between the LAB and the MLD which are usually petrologically interpreted very differently (e.g., Yuan and Romanowicz, 2010). The similarity of the seismic appearance of the phanerozoic LAB and the cratonic MLD was confirmed across the TTZ by Knapmeyer-Endrun et al. (2017). We also note that Moho, LAB and SLD are shallowing beneath the Pannonian Basin (Fig. 6C and D).

Below the SLD signal, near 300 km depth we see in Fig. 6C and D a blue signal indicating velocity increase downward and marked as Lehmann discontinuity. The X discontinuity of Shen et al. (2014) agrees relatively well with our Lehmann discontinuity. This signal is observed frequently on a global scale and interpreted as bottom of the asthenosphere or as caused by anisotropy (Lehmann, 1959; Gu et al., 2001). The strong observation of this discontinuity in S-receiver functions argues against a change in azimuthal anisotropy. S-receiver functions are P-waves therefore with no transverse component in the isotropic and homogeneous case. We did not observe clear azimuthal variations of the amplitudes of the converted P-waves. Also the discrimination between effects of anisotropy and heterogeneity would not be easy. A rare positive example of anisotropy observations in S-receiver functions is

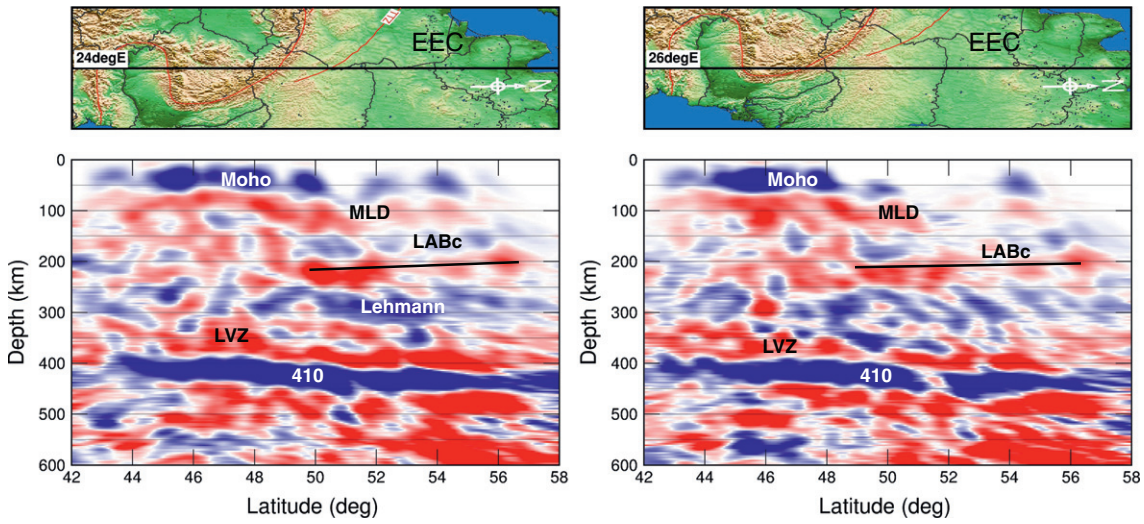

Fig. 7. Two north-south profiles showing the possible connection between the SLD and the cratonic LAB (marked LABc) across the boundary between the East European Craton and Phanerozoic Europe.

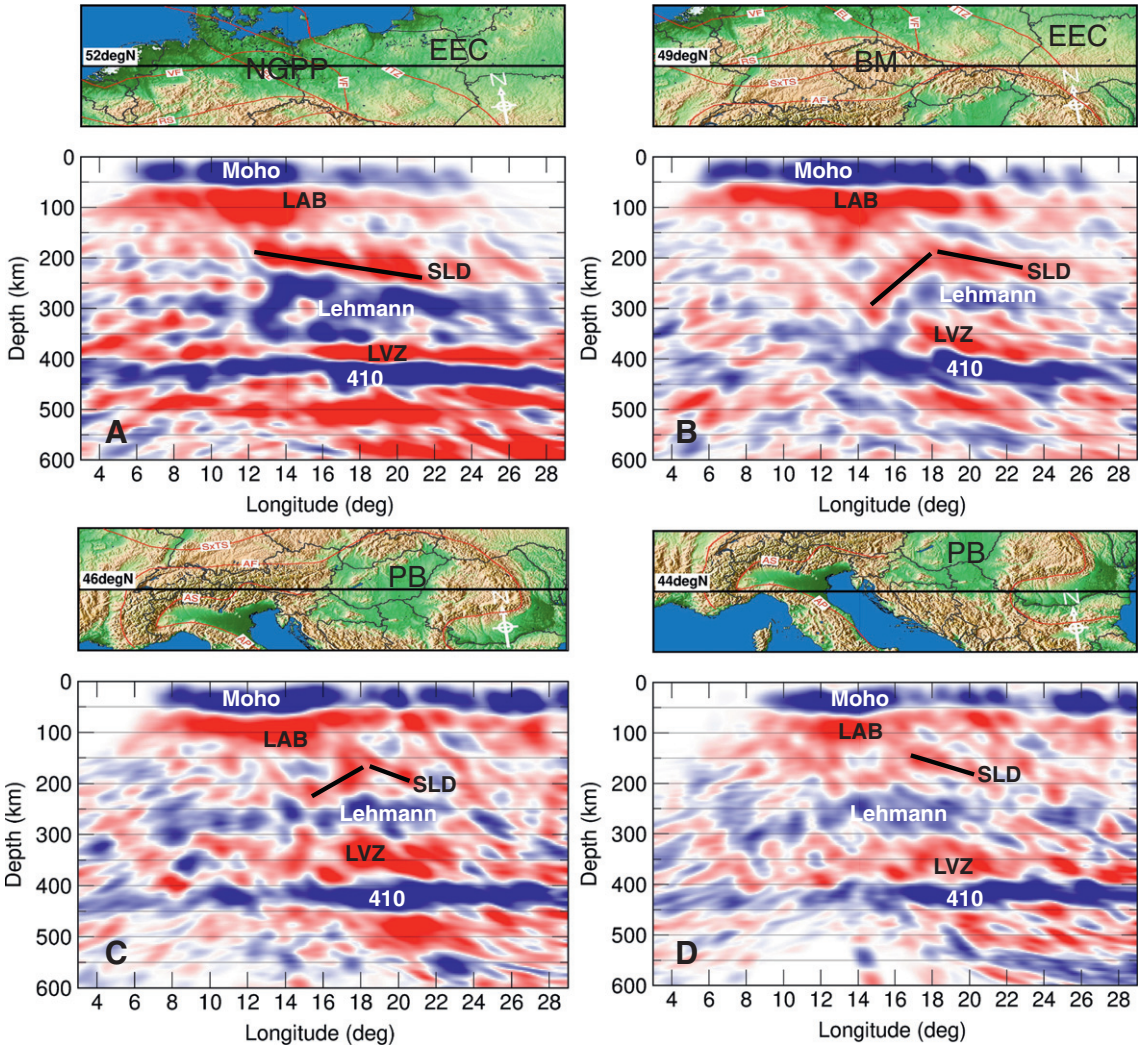

Fig. 8. Four east-west profiles through the upper mantle at 52°N (A), 49°N (B), 46°N (C) and 44°N (D). (A) The cratonic LABc seems to reach westward beyond the Tornquist-Teisseyre Zone to the Elbe Line (marked SLD). (B) The signal SLD below the Bohemian Massif is dipping steeply to the west down to 300 km. To the east, the SLD is connected with SLD west of the TTZ. This is in contrast to Fig. 4A and B where the SLD is laterally discontinuous. The LABp in (C) and (D) is the LAB of the Adriatic microplate. More east-west profiles are shown in Fig. S1 in the Supplementary material.

given by Sodoudi et al. (2013) in South Africa where the sign of the conversion reverses with backazimuth. Between the Lehmann and the 410 discontinuities we observe another red discontinuity (top of a low velocity zone) marked LVZ. This is a relatively global discontinuity (e.g., Tauzin et al., 2010), probably caused by an increased presence of water (Bercovici and Karato, 2003).

Fig. 8 shows four east-west profiles. The profile in Fig. 8A at 52°N shows clearly the negative discontinuity at 200 km depth below the region east of the Elbe Line which is marked SLD. In Fig. 8A we see also the Phanerozoic LAB and the MLD above the SLD signal. The Profile in Fig. 8B shows a very different structure than in Fig. 8A. The SLD signal is horizontal at 200 km depth north-east of the Bohemian Massif. Below the Bohemian Massif SLD is west dipping to 300 km depth. Fig. 6A and B and Fig. 8B show that the inclination of the SLD signal below the Bohemian Massif has a north and a west component, which means it is dipping towards the north-west. In Fig. 8C and D are shown two east-west profiles along 44 and 46°N latitude, crossing the northern edge of the Adria towards the Pannonian Basin. Both profile show only weak indication of the SLD structure. This is probably because the main dip of SLD is towards the north, perpendicular to the profile.

Fig. 9 shows a map of the depth distribution of the newly observed SLD signal derived from the north-south profiles. The according data are shown in detail in Fig. S2 and listed in Table S2 in the Supplementary material. The according plot derived from east-west profiles is shown in Fig. S1 in the Supplementary material with depth values listed in TableS1. The agreement of the depth maps of SLD derived from the two sets of profiles is in some regions poor. Differences of >40 km are marked in Fig. 9 with plus or minus signs. Plus signs indicate that the depth derived from north-south profiles is greater and minus signs indicate greater depth at east-west profiles. These regions are concentrated at the Bohemian Massif and the Pannonian Basin. In all other regions the agreement is relatively good. That means that the upper mantle below the BM and the PB is especially complicated and difficult to image with our data. Our profiles are 400 km wide and therefore in a complex region east-west and north-south profiles do not show necessarily the same depth at the same location. Narrower profiles would be needed to resolve such complicated regions which would require denser station distribution. We think we can estimate from our data that the SLD discontinuity is dipping roughly to the north-west to a depth of about 300 km below the Bohemian Massif and probably continues at 200 km depth below the North German-Polish Basin. The SLD shallows from the Bohemian Massif to about 150 km depth towards the Pannonian Basin. Below the Pannonian Basin we estimate that the SLD discontinuity deepens roughly towards the north from about 150 km to 250 km below the East European Craton (see Fig. S2).

5. Discussion and conclusions

5.1. North German-Polish Plain

An important observation in our study is the LAB of the East European Craton near 200 km depth. The question if the cratonic LAB can be observed with converted waves is still controversial. It is relevant for the question if this discontinuity is caused by temperature alone or if an additional or a different mechanism is required. Converted waves can only be generated at a relatively sharp discontinuity which would argue against a pure temperature effect. For example, Hopper and Fischer (2015) did not observe the LAB in S-receiver functions below the cratonic North America. In contrast to that, Kind et al. (2015a) observed at least indications of the cratonic LAB there. Good evidence for the existence of the cratonic LAB was found by Kind et al. (2013) beneath Scandinavia. Now we found also evidence for a relative sharp LAB below the East European Craton. In addition it seems likely that the observed SLD is a westerly extension of the cratonic LAB to about the Elbe Line. In tomography the western boundary of the intact EEC is observed at the Tornquist-Teisseyre Zone (e.g., Legendre et al., 2012). However, Legendre et al. (2012) also found indications of a transition zone between the EEC and Phanerozoic Europe reaching from the TTZ to the Elbe Line. Gossler et al. (1999) found evidence in P-receiver functions beneath the North German and Danish Basin for an extension of the Baltica lower crust to the Elbe Line. Dadlez et al. (2005) used large-scale seismic refraction and wide angle reflection technique to study the TTZ. They assumed that the lower and middle crust below the Polish Basin consist of terranes built of EEC crust. Mazur et al. (2015) also found evidence in an integrated gravity, magnetic and seismic study for the extension of the middle and lower crust of the EEC towards the Elbe line.

There is also independent evidence for an extension of the EEC lower crust towards the Elbe Line. Breitkreuz and Kennedy (1999) and Breitkreuz et al. (2007) studied SHRIMP U-Pb ages from zircon cores of inherited zircon grains, derived from Upper Carboniferous to Lower Permian volcanic rocks from drill cores of the Central European Basin System. About seventy of their analyses represent Avalonia and subordinately southern EEC crust. Pietranik et al. (2013) continues this research by study of the O- and Hf-isotope composition of inherited rhyolitic zircons from drill cores across the North German Basin and found that sediments and basement beneath the NE German Basin are part of EEC. Independent from seismic and seismologic data this result also confirms Baltica lower crust there. All these findings including our own results lead to the conclusion that the Elbe Line is the western boundary of a transition zone between the East European Craton and Phanerozoic Europe in the mantle lithosphere. In this transition zone below the Phanerozoic LAB a prong of the cratonic lithosphere may extend towards the south-west of the Tornquist-Teisseyre Zone. Also the shear-wave velocity model for this region (green model, Fig. 3D) indicates enlarged shear-wave velocities at depth between 230 km and 270 km comparable to those in the cratonic mantle lithosphere. Knapmeyer-Endrun et al. (2013) interpreted the increase of the shear-wave velocity beneath the asthenosphere as indication for small-scale convection and downward directed corner flow. In conclusion, there is evidence from surface wave tomography, lower crustal seismics, petrology and receiver functions that the mantle lithosphere and the lower crust between about the Tornquist-Teisseyre Zone and the Elbe Line are related to the East European Craton.

5.2. Bohemian Massif

Another significant new observation is the existence of a structure below the Bohemian Massif which dips towards its north-western edge to 300 km depth (SLD signals in Fig. 6A and B and Fig. 8B). We note that the Phanerozoic LAB is located at a depth of about 100–120 km, placing the SLD in the upper mantle below the LAB. The LAB was found in the northern part of the Bohemian Massif at 80–90 km depth in a study based on anisotropy observations (Plomerova and Babuska, 2010). A shorter period S-receiver function study found the LAB deepening to the south from about 60 to 140 km depth (Heuer et al., 2007) in reasonable agreement with our present longer period observations (Figs. 6 and 8).

New discoveries about the origin of microdiamond and coesite bearing ultrahigh pressure metamorphic (UHMP) rocks are taken as evidence for continental subduction, collision and exhumation from depths of >100–250 km, associated with the Variscan orogeny (Dobrzhinetskaya and Faryad, 2011; Perraki and Faryad, 2014). Both minerals have been found as inclusions in garnet and zircon in UHMP rocks, occurring at the surface or near the surface in the northern and central part of the Bohemian Massif:

(1) Saxothuringian Zone, Erzgebirge/Germany: Seidenbach gneiss, size of ~1–50 μm (Massonne, 1999), age: 337 Ma (Massonne et al., 2007) and the Eger Graben area/Czech Republic: kyanite-bearing eclogite in the T-38 borehole (Kotkova et al., 2011);

(2) Moldanubian Zone, Kutna Hora Complex/Czech Republic: felsic granulites (Perraki and Faryad, 2014) and orogenic spinel-garnet peridotite, size of ~5 μm, age: 340–350 Ma, (Naemura et al., 2011).

Dobrzhinetskaya et al. (2010) studied carbon isotope ratios in microdiamonds from Erzgebirge and obtained $\delta^{13}C$ ratios belonging to biogenic matter (between −25.5‰ and −17.8‰). This confirms deep subduction of continental crustal sediments. Stöckhert et al. (2009) reasoned that the decompression rate must have been extremely high and suggest minimum exhumation rate in the order of 100 m/year, which corresponds to ascent rates of magma. According to Babuska and Plomerova (2013) the collisional mantle boundaries served as major exhumation channels of the HMP and UHMP rocks. Magmatic equilibration (Oncken, 1998) indicates a detachment of the slab after the collision.

However, it is unlikely or not clear if a Variscan slab is causing the SLD discontinuity beneath the Bohemian Massif because of the northward drift of Eurasia after collision and the thermal equilibration of the slab. Recent tomographic images show no indication of a plume or subduction below the Bohemian Massif (Plomerova et al., 2016). Vecsey et al. (2014) concluded from anisotropy observations that the mantle lithosphere of the East European Craton might extend westward to the Bohemian Massif. Further analyses are needed to clarify seismologic, rheological, petrologic and tectonic origin of the upper mantle underneath the Bohemian Massif.

5.3. Alps and Pannonian Basin

Indications of subduction are observed below the Alps (Fig. 4 and Fig. S2, slides 3 and 4). The south-east subduction direction of the European lithosphere below the central Alps is confirmed by our data.

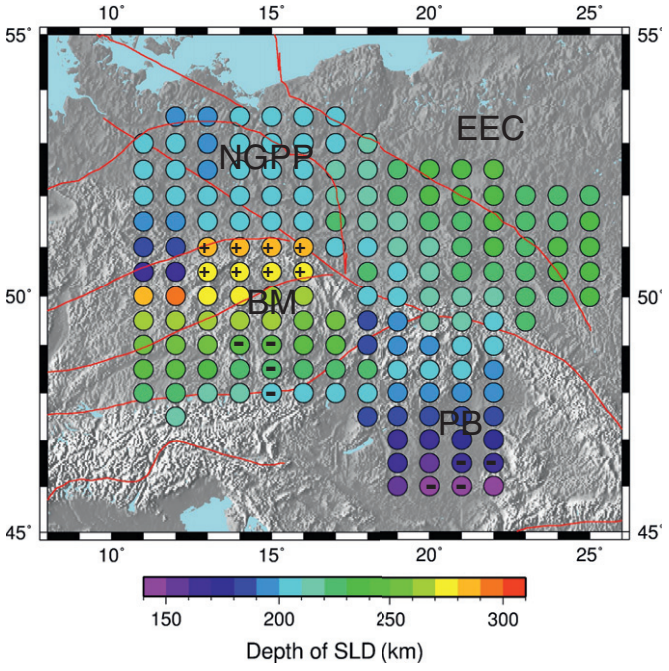

Fig. 9. Map of the depth of the SLD discontinuity obtained from the north-south profiles. All these profiles are shown in Fig. S2 in the Supplementary material with depth readings of the SLD discontinuity marked. The readings itself are shown in Table S2 also in the Supplementary material. Plus and minus signs indicated locations where the difference of the SLD depth between north-south profiles and east-west profiles is >40 km. Plus signs indicate greater depths in the north-south profiles and minus signs smaller depths than in the east-west profiles. All data of the east-west profiles are given in Fig.S1 and TableS1 in the Supplementary material. See Fig. 1 for tectonic units.

The resolution of our data is, however, not high enough for a clear observation of the subduction direction in the eastern Alps. The depth penetration is near 150 km, which is close to the results obtained from Lippitsch et al. (2003) in their teleseismic P-wave tomography. Already Babuska et al. (1990) previously suggested a polarity change between eastern and western Alps from P residual observations.

Below the Pannonian Basin we observed shallowing of the Moho and the Phanerozoic LAB. However, beneath the LAB we observed a second negative discontinuity. This discontinuity is also marked SLD like the one below the Bohemian Massif. It seems closely related to the SLD of the Bohemian Massif (see Fig. 4), however it does not have the step at the northern end but changes gradually into the LAB of the EEC. It deepens from about 150 km depth at the south-western edge of the Pannonian Basin to about 200 km depth beneath the western Carpathians (see Fig. 7). Therefore we think that the SLD structure below the PB may be related to the edge of the EEC rather than to a European (Alpine-Carpathian) or Dinaric (Adriatic) slab, especially since Miocene European subduction in the Carpathians was to the S and SE (away from the Bohemian massif) and Paleogene NE-directed shortening in the Dinarides was far too small in the vicinity of the slab gap between 44 and 46°N (e.g., Spakman and Wortel, 2004; Handy et al., 2015). Wortel and Spakman (2000) imaged a slab within the mantle transition zone (MTZ) below the Pannonian Basin. The structures discussed here are well above the MTZ.

5.4. Phanerozoic LAB and cratonic MLD

We have also interesting observations of the Phanerozoic LAB and the cratonic MLD. Their seismic signature and their depth do not change significantly across very different tectonic units. The petrophysical nature of the MLD is, for example, discussed by Hopper and Fischer (2015) or by Rader et al. (2015). The suggestion of Rader et al. (2015) that the MLD is the inactive remnant of fossil LAB seems in good agreement with the identical receiver function image of both discontinuities. Their model describes a gradual lateral transition from the original shallow LAB of the active cratonic margin to the cratonic MLD.

5.5. Final conclusions

We think we have shown that the S-receiver function technology is an excellent method to illuminate the region between Moho and upper mantle transition zone, especially in connection with surface wave tomography. Results of tomography and S-receiver functions agree not completely (see Fig. 5). Unknown discontinuities may be discovered with S-receiver functions which could be very important for understanding more details of plate collision. A limitation of the method is that the signals used are usually below the noise level and must be made visible by summation of many records. Since large regions of piercing point distribution are needed, the lateral resolution is limited if the station coverage is not dense enough. Also the recording period should be long enough to collect a sufficient number of events. Permanent stations are certainly most useful.

The most significant property of the newly discovered SLD in the neighborhood of the East European Craton but still below the Phanerozoic part of Europe is its connection to the LAB of the East European Craton. The observed northwest and northeast dipping SLD structures below the Bohemian Massif and the Pannonian Basin, respectively, are difficult to reconcile with current knowledge of circum-Carpathian subduction of European lithosphere, which dipped towards the Pannonian Basin and away from the Bohemian Massif in Miocene time. A preliminary interpretation of these features is that a prong of the cratonic mantle lithosphere penetrated into the Phanerozoic asthenosphere during the continental collision at the western and south-western edges of the EEC.

The observation of waves converted at the SLD which is about 10 km sharp (Fig. 3) excludes the option that temperature effects are its only

cause. If the SLD is considered a continuation of the cratonic LAB it could be the chemical boundary layer at the bottom of the melt-depleted and dehydrated peridotites in Jordan's (1978) tectosphere model (see also Lee et al., 2011 and citations therein). However, only more seismologic, petrologic and geochemic data could resolve more precisely the rheology, structure and evolution of the upper mantle there. This is especially necessary in the regions of the Bohemian Massif, the eastern Alps and the Pannonian Basin.

Supplementary data to this article can be found online at http://dx.doi.org/10.1016/j.tecto.2017.02.002.

Acknowledgements

We appreciate of the open data policy of the international seismology organizations which permits easy mining in data archives. We also appreciate the high quality of the permanent observatory broadband stations. By far most data used in our study came from permanent stations. We would like to thank all the data providers who made their data openly available. These data providers are: Seismic Network of the Republic of Slovenia-**SL;** MEDNET Project, Rome, Italy-**MN;** Czech Regional Seismological Network-**CR;** Austrian Seismic Network-**OE;** Hungarian National Seismological Network-**HU;** GEOFON Program, GFZ Potsdam, Germany-**GE;** Slovak National Network of Seismic Stations-**SK;** Swiss Seismological Network-**CH;** GEOSCOPE French Global Seismological Network of Broadband Stations-**G;** TRANSALP Project Friuli/Veneto 2002-2004, GFZ Potsdam-**ZO;** RESIF/SISMOB mobile antenna-**Y4;** CEA/DASE broadband permanent network (RESIF)-**RD;** RESIF and other broadband networks-**FR;** IGG Seismic Network Genova-**GU;** Italian Seismic Network-**IV;** Universita della Basilicata-**BA;** Thuringia Seismic Net, Uni Jena, Germany-**TH**, Bayernnetz, Germany-**BW**, German Regional Seismic Network, BGR Hannover-**GR;** Serbian Network of Seismic Stations-**SJ;** Saxonia Seismic Network, Uni Leipzig, Germany-**SX**; Polish Seismic Network-**PL;** Czech Regional Seismic Network-**CZ;** NE Italy broadband Network-**NI;** MIDSEA Temporary Network-**YF;** Hellenic Seismic Network-**HL**; Aristotle University Thessaloniki-**HT;** Romanian Seismic Network-**RO;** Bulgaria Seismic Network-**BS;** TOR Temporary GEOFON Network-**ZA;** Passeq Project 2006/2008,Univ. Warsaw-**7E;** Danish National Seismic Network-**DK;** BOHEMA Project 2002/03 GFZ Potsdam-**ZV;** JULS Project 2010/11, GFZ Potsdam-**ZW;** Our special thanks to the responsible persons in Rome and Wolfgang Lenhardt in Vienna for making the restricted Südtirol-**SI** data available to us. All data have been obtained through the EIDA portal.

We also wish to thank the Working Groups PASSEQ (Wilde-Piorko et al., 2008), BOHEMA (Plomerova et al., 2003), JULS (Kind et al., 2013) and TOR (TOR Working Group, 1999) for making their data also available. Finally we thank an anonymous reviewer and Jarka Plomerova for careful reviews and numerous significant suggestions to improve the manuscript.

References

Alinaghi, A., Bock, G., Kind, R., Hanka, W., Wylegalla, K., TOR and SVEKALAPKO Working Groups, 2003. Receiver function analysis of the crust and upper mantle from the North German Basin to the Archaen Baltic Shield. Geophys. J. Int. 155, 641–652.

Auer, L., Boschi, L., Becker, T.W., Nissen-Meyer, T., Giardini, D., 2014. Savani: A variable-resolution whole-mantle model of anisotropic shear-velocity variations based on multiple datasets. J. Geophys. Res. Solid Earth 119.

BABEL Working Group, 1990. Evidence for early Proterozoic plate tectonics from seismic reflection profiles in the Baltic Shield. Nature 348, 34–38.

Babuska, V., Plomerova, J., 2013. Boundaries of mantle-lithosphere domains in the Bohemian Massif as extinct exhumation channels for high-pressure rocks. Gondwana Res. 23, 973–987.

Babuska, V., Plomerova, J., Granet, M., 1990. The Deep Lithosphere in the Alps: A Model Inferred From P Residuals. Vol. 176 pp. 137–165.

Balling, N., 2000. Deep seismic reflection evidence for ancient subduction and collision zones within the continental lithosphere of northwestern Europe. Tectonophysics 329, 269–300.

Bartzsch, S., Lebedev, S., Meier, T., 2011. Resolving the lithosphere-asthenosphere boundary with seismic Rayleigh waves. Geophys. J. Int. 186 (3), 1152–1164.

Bayer, U., Grad, M., Pharaoh, T.C., Thybo, H., Guterch, A., Banka, D., Lamarche, J., Lassen, A., Lewerenz, B., Scheck, M., Marotta, A.M., 2002. The southern margin of the East European Craton: new results from seismic sounding and potential fields between the North Sea and Poland. Tectonophysics 360 (1–4), 301–314.

Bercovici, D., Karato, S.-I., 2003. Whole-mantle convection and the transition-zone water filter. Nature 425 (6953), 39–44.

Bianchi, I., Miller, M.S., Bokelmann, G., 2014. Insights on the upper mantle beneath the Eastern Alps. Earth Planet. Sci. Lett. 403, 199–209.

Bijwaard, H., Spakman, W., 2000. Non-linear global P-wave tomography by iterated linearized inversion. Geophys. J. Int. 141 (1), 71–82.

Bostock, M.G., 1998. Mantle stratigraphy and evolution of the Slave province. J. Geophys. Res. 103 (B9), 21 (183–21,200).

Breitkreuz, C., Kennedy, A., 1999. Magmatic flare-up at the Carboniferous/Permian boundary in the NE German Basin revealed by SHRIMP zircon ages. Tectonophysics 302, 307–326.

Breitkreuz, C., Kennedy, A., Geißler, M., Ehling, B.-C., Kopp, J., Muszynski, A., Protas, A., Stouge, S., 2007. Far Eastern Avalonia: its chronostratigraphic structure revealed by SHRIMP zircon ages from Upper Carboniferous to Lower Permian volcanic rocks (drill cores from Germany, Poland, and Denmark). GSA Special Papers 2007 (423), 173–190.

Dadlez, R., Grad, M., Guterch, A., 2005. Crustal structure below the Polish Basin: is it composed of proximal terranes derived from Baltica? Tectonophysics 411, 111–128.

Dobrzhinetskaya, L.F., Faryad, S.W., 2011. Frontiers of ultrahigh-pressure metamorphism: view from field and laboratory. In: Dobrzhinetskaya, L., Faryad, S.W., Wallis, S., Cuthbert, S. (Eds.), Ultrahigh-pressure Metamorphism: 25 Years After Discovery of Coesite and Diamond. Elsevier, pp. 1–39.

Dobrzhinetskaya, L.F., Green, H.W., Takahata, N., Sano, Y., Shirai, K., 2010. Crustal signature of $\delta^{13}C$ and nitrogen content in microdiamonds from Erzgebirge, Germany, in microprobe studies. J. Earth Sci. 21, 623–634.

Dueker, K.G., Sheehan, A.F., 1997. Mantle discontinuity structure from midpoint stacks of converted P to S waves across the Yellowstone hotspot track. J. Geophys. Res. 102, 8313–8327.

Faccenna, C., et al., 2014. Mantle dynamics in the Mediterranean. Rev. Geophys. 52: 283–332. http://dx.doi.org/10.1002/2013RG000444.

Franke, W., 2000. The mid-European segment of the Variscides: tectonostratigraphic units, terrane boundaries and plate tectonic evolution. In: Franke, W., Haak, V., Oncken, O., Tanner, D. (Eds.), Orogenic Processes: Quantification and Modelling in the Variscan Belt. Geological Society [London] Special Publication Vol. 179, pp. 35–61.

Franke, W., 2014. Topography of the Variscan orogen in Europe: failed-not collapsed. Int. J. Earth Sci. 103, 1471–1499.

Geissler, W.H., Kind, R., Yuan, X., 2008. Upper mantle and lithospheric heterogeneities in central and eastern Europe as observed by teleseismic receiver functions. Geophys. J. Int. 174, 351–376.

Geissler, W.H., Sodoudi, F., Kind, R., 2010. Thickness of the central and eastern European lithosphere as seen by S receiver functions. Geophys. J. Int. 181, 604–634.

Geissler, W.H., Kämpf, H., Skacelova, Z., Plomerova, J., Babuska, V., Kind, R., 2012. Lithosphere structure of the NE Bohemian Massif (Sudetes)—a teleseismic receiver function study. Tectonophysics 564–565, 12–37.

Giacomuzzi, G., Chiarabba, C., De Gori, P., 2011. Linking the Alps and Apennines subduction systems: new constraints revealed by high-resolution teleseismic tomography. Earth Planet. Sci. Lett. 301, 531–543.

Gossler, J., Kind, R., Sobolev, S., Kämpf, H., Wylegalla, K., Stiller, M., TOR Working Group, 1999. Major crustal features between the Harz Mountains and the Baltic Shield derived from receiver functions. Tectonophysics 314, 321–333.

Grad, M., Tiira, T., ESC Working Group, 2009. The Moho depth map of the European Plate. Geophys. J. Int. 176 (1), 279–292.

Gu, Y.J., Dziewonski, A.M., Ekström, G., 2001. Preferential detection of the Lehmann discontinuity beneath continents. Geophys. Res. Lett. 28 (24), 4655–4658.

Gutenberg, B., 1926. Untersuchungen zur Frage bis zu welcher Tiefe die Erde kristallin ist. Z. Geophys. 2, 24–29.

Handy, M.R., Ustaszewski, K., Kissling, E., 2015. Reconstructing the Alps–Carpathians–Dinarides as a key to understanding switches in subduction polarity, slab gaps and surface motion. Int. J. Earth Sci. 104 (1), 1–26.

Heuer, B., Geissler, W.H., Kind, R., Kämpf, H., 2006. Seismic evidence for asthenospheric updoming beneath the western Bohemian Massif, central Europe. Geophys. Res. Lett. 33.

Heuer, B., Kämpf, H., Kind, R., Geissler, W.H., 2007. Seismic evidence for whole lithosphere separation between Saxothuringian and Moldanubian tectonic units in central Europe. Geophys. Res. Lett. 34.

Heuer, B., Geissler, W.H., Kind, R., BOHEMA working group, 2011. Receiver function search for a baby plume in the mantle transition zone beneath the Bohemian Massif. Geophys. J. Int. 187, 577–594.

Hopper, E., Fischer, K.M., 2015. The meaning of the midlithospheric discontinuities: a case study in the northern U.S. craton. Geochem. Geophys. Geosyst. 16.

Hrubcova, P., Geissler, W.H., 2009. The crust-mantle transition and the Moho beneath the Vogtland/West Bohemian region in the light of different seismic methods. Stud. Geophys. Geod. 53, 275–294.

Jones, C.H., Phinney, R.A., 1998. Seismic structure of the lithosphere from teleseismic converted arrivals observed at small arrays in the southern Sierra Nevada and vicinity, California. J. Geophys. Res. 103, 10065–10090.

Jones, A.G., Plomerova, J., Korja, T., Sodoudi, F., Spakman, W., 2010. Europe from the bottom up: a statistical examination of the central and northern European lithosphere-asthenosphere boundary from comparing seismological and electromagnetic observations. Lithos 120, 14–29.

Jordan, T.H., 1978. Composition and development of the continental tectosphere. Nature 274, 544–548.
Karato, S.-i., Olugboji, T., Park, J., 2015. Mechanisms and geological significance of the mid-lithospheric discontinuity in the continents. Nat. Geosci. 8, 509–514.
Karousova, H., Plomerova, J., Babuska, V., 2013. Upper-mantle structure beneath the southern Bohemian Massif and its surroundings imaged by high-resolution tomography. Geophys. J. Int. 194, 1203–1215.
Kennett, B.L.N., Engdahl, E.R., 1991. Travel times for global earthquake location and phase identification. Geophys. J. Int. 105, 429–465.
Kennett, B.L.N., Engdahl, E.R., Buland, R., 1995. Constraints on seismic velocities in the Earth from traveltimes. Geophys. J. Int. 122, 108–124.
Kind, R., 1985. The reflectivity method for different source and receiver structures. J. Geophys. 58, 146–152.
Kind, R., Yuan, X., Kumar, P., 2012. Seismic receiver functions and the lithosphere-asthenosphere boundary. Tectonophysics 536–537, 25–43.
Kind, R., Sodoudi, F., Yuan, X., Shomali, H., Roberts, R., Gee, D., Eken, T., Bianchi, M., Tilmann, F., Balling, N., Jacobsen, B.H., Kumar, P., Geissler, W.H., 2013. Scandinavia: a former Tibet? Geochem. Geophys. Geosyst. 14, 4479–4487.
Kind, R., Yuan, X., Mechie, M., Sodoudi, F., 2015a. Structure of the upper mantle in the north-western and central United States from USArray S-receiver functions. Solid Earth 6, 957–970.
Kind, R., Eken, T., Tilmann, F., Sodoudi, F., Taymaz, T., Bulut, F., Yuan, X., Can, B., Schneider, F., 2015b. Thickness of the lithosphere beneath Turkey and surroundings from S-receiver functions. Solid Earth 6, 971–984.
Knapmeyer-Endrun, B., Krüger, F., Legendre, C.P., Geissler, W.H., PASSEQ Working Group, 2013. Tracing the influence of the Trans-European Suture Zone into the mantle transition zone. Earth Planet. Sci. Lett. 363, 73–87.
Knapmeyer-Endrun, B., Krüger, F., Geissler, W.H., PASSEQ Working Group, 2017. Upper mantle structure across the Trans-European Suture Zone imaged by S-receiver functions. Earth Planet. Sci. Lett. 458, 429–441.
Kosarev, G., Kind, R., Sobolev, S.V., Yuan, X., Hanka, W., Oreshin, S., 1999. Seismic evidence for detached Indian lithospheric mantle beneath central Tibet. Science 283, 1306–1308.
Kotkova, J., O'Brien, P.J., Ziemann, M., 2011. Diamond and coesite discovered in Saxonytype granulite: solution to the Variscan garnet peridotite enigma. Geology 39, 667–670.
Koulakov, I., Kaban, M., Tesauro, M., Cloetingh, S., 2009. P- and S-velocity anomaly in the upper mantle beneath Europe from tomographic inversion of ISC data. Geophys. J. Int. 179, 345–366.
Kroner, U., Romer, R.L., 2013. Two plates — many subduction zones: the Variscan orogeny reconsidered. Gondwana Res. 24, 298–329.
Kummerow, J., Kind, R., Oncken, O., Giese, P., Ryberg, T., Wylegalla, K., Scherbaum, F., TRANSALP Working Group, 2004. A natural and controlled source seismic profile through the Eastern Alps: TRANSALP. Earth Planet. Sci. Lett. 225, 115–129.
Lee, C.-T.A., Lu, P., Chin, E.J., 2011. Building and destroying continental mantle. Annu. Rev. Earth Planet. Sci. 39, 59–90.
Legendre, C.P., Meier, T., Lebedev, S., Friederich, W., Viereck-Götte, L., 2012. A shear wave velocity model of the European upper mantle from automated inversion of seismic shear and surface waveforms. Geophys. J. Int. 191, 282–304.
Lehmann, I., 1959. Velocities of longitudinal waves in the upper part of the earth's mantle. Ann. Geophys. 15 (1), 93–118.
Linnemann, U., 2007. Ediacaran rocks from the Cadomian basement of the Saxo-Thuringian Zone (NE Bohemian Massif, Germany): age constraints, geotectonic setting and basin development. In: Vickers-Rich, Komarower, P. (Eds.), The Rise and Fall of the Ediacaran Biota. Geological Society [London] Special Publications Vol. 286, pp. 35–51.
Lippitsch, R., Kissling, E., Ansorge, J., 2003. Upper mantle structure beneath the Alpine orogen from high-resolution teleseismic tomography. J. Geophys. Res. 1088 (B8), 2376.
Lombardi, D., Braunmiller, J., Kissling, E., Giardini, D., 2008. Moho depth and Poisson's ratio in the Western–Central Alps from receiver functions. Geophys. J. Int. 173, 249–264.
Lombardi, D., Braunmiller, J., Kissling, E., Giardini, D., 2009. Alpine mantle transition zone imaged by receiver functions. Earth Planet. Sci. Lett. 278, 163–174.
Marquering, H., Snieder, R., 1996. Shear-wave velocity structure beneath Europe, the northeastern Atlantic and western Asia from waveform inversions including surface-wave mode coupling. Geophys. J. Int. 127, 283–304.
Massonne, H.-J., 1999. A new occurrence of microdiamonds in quartzofeldspathic rocks of the Saxonian Erzgebirge, Germany, and the metamorphic evolution. In: Gurney, J.J., Gurney, J.L., Pascoe, M.D., Richardson, S.H. (Eds.), The P.H. Nixon Volume. Proceedings of 7th International Kimberlitic Conference. Red Roof Design CC, Capetown, pp. 533–539.
Massonne, H.J., Kennedy, A., Nasdala, L., Theye, T., 2007. Dating of zircon and monazite from diamondiferous quartzofeldspathic rocks of the Saxonian Erzgebirge. Mineral. Mag. 71, 407–425.
Matte, Ph., 1998. Continental subduction and exhumation of HP rocks in Paleozoic orogenicbelts: Uralides and Variscides. 120. GFF, Stockholm, pp. 209–222.
Mazur, S., Mikolajczak, M., Krzywiec, P., Malinowski, M., Buffenmyer, V., Lewandowski, M., 2015. Is the Teisseyre-Tornquist Zone an ancient plate boundary of Baltica? Tectonics 34, 2465–2477.
Meier, T., Dietrich, K., Stöckhert, B., Harjes, H.-P., 2004. One-dimensional models of shear-wave velocity for the eastern Mediterranean obtained from the inversion of Rayleigh wave phase velocities and tectonic implications. Geophys. J. Int. 156, 45–58.
Meier, T., Soomro, R.A., Viereck, L., Lebedev, S., Behrmann, J.H., Weidle, C., Cristiano, L., Hanemann, R., 2016. Mesozoic and Cenozoic evolution of the Central European Lithosphere. Tectonophysics 692, 58–73.
Meissner, R., Rabbel, W., 1999. Nature of crustal reflectivity along the DEKORP profiles in Germany in comparison with reflection patterns from different tectonic units worldwide: a review. Pure Appl. Geophys. 156, 7–28.
Mierdel, K., Keppler, H., Smyth, J.R., Falko, L., 2007. Water solubility in aluminous orthopyroxene and the origin of Earth's asthenosphere. Science 315, 364–368.
Miller, M.S., Piana Agostinetti, N., 2012. Insights into the evolution of the Italian lithospheric structure from S receiver function analysis. Earth Planet. Sci. Lett. 348, 49–59.
Mitterbauer, U., Behm, M., Brückl, E., Lippitsch, R., Guterch, A., Keller, G.R., Koslovskaya, E., Rumpfhuber, E.-M., Sumanovac, F., 2011. Shape and origin of the east-Alpine slab constrained by the ALPASS teleseismic model. Tectonophysics 510, 195–206.
Naemura, K., Ikuta, D., Kagi, H., Odake, S., Ueda, T., Ohi, S., Kobayashi, T., Svojtka, M., Hirajima, T., 2011. Diamond and other possible ultradeep evidence discovered in the orogenic spinel-garnet peridotite from the Moldanubian Zone of the Bohemian Massif, Czech Republic. In: Dobrzhinetskaya, L., Faryad, S.W., Wallis, S., Cuthbert, S. (Eds.), Ultrahigh-pressure Metamorphism, 25 Years After the Discovery of Coesite and Diamond. Elsevier, pp. 77–111.
Nance, R.D., Linnemann, U., 2008. The Rheic Ocean: origin, evolution, and significance. GSA Today 18, 4–12.
Oncken, O., 1998. Evidence for precollisional subduction erosion in ancient collisional belts; the case of the mid-European Variscides. Geology 26 (12), 1075–1078.
Perraki, M., Faryad, S.W., 2014. First finding of microdiamond, coesite and other UHP phases in felsic granulites in the Moldanubian Zone: implications for deep subduction and a revised geodynamic model for Variscan Orogeny in the Bohemian Massif. Lithos 202–203, 157–166.
Pietranik, A., Słodczyk, E., Hawkesworth, C.J., Breitkreuz, C., Storey, C.D., Whitehouse, M., Milke, R., 2013. Heterogeneous zircon cargo in voluminous late Paleozoic rhyolites: Hf, O isotope and Zr/Hf records of plutonic to volcanic magma evolution. J. Petrol. 54 (8), 1483–1500.
Piromallo, C., Morelli, A., 2003. P-wave tomography of the mantle under the Alpine–Mediterranean area. J. Geophys. Res. 108 (B2).
Plomerova, J., Babuska, V., 2010. Long memory of mantle lithosphere fabric — European LAB constrained from seismic anisotropy. Lithos 120 (1–2), 131–143.
Plomerova, J., Achauer, U., Babuska, V., Granet, M., BOHEMA Working Group, 2003. Passive seismic experiment to study lithosphere–asthenosphere system in the western part of the Bohemian Massif. Stud. Geophys. Geod. 47, 691–701.
Plomerova, J., Munzarova, H., Vecsey, L., Kissling, E., Achauer, U., Babuska, V., 2016. Cenozoic volcanism in the Bohemian Massif in the context of P- and S-velocity high-resolution teleseismic tomography of the upper mantle. Geochem. Geophys. Geosyst. 17: 3326–3349. http://dx.doi.org/10.1002/2016GC006318.
Rabbel, W., Forste, K., Schulze, A., Bittner, R., Rohi, J., Reichert, J.C., 1995. A high-velocity layer in the lower crust of the North German Basin. Terra Nova 7, 327–337.
Rader, E., Emry, E., Schmerr, N., Frost, D., Cheng, C., Menard, J., Yu, C.-Q., Geist, D., 2015. Characterization and petrological constraints of the midlithospheric discontinuity. Geochem. Geophys. Geosyst. 16, 3484–3504.
Schmid, S.M., Fügenschuh, B., Kissling, E., Schuster, R., 2004. Tectonic Map and overall architecture of the Alpine orogen. Eclogae Geol. Helv. 97 (1), 93–117.
Schneider, F.M., Yuan, X., Schurr, B., Mechie, J., Sippl, C., Haberland, C., Minaev, V., Oimahmadov, I., Gadoev, M., Radjabov, N., Abdybachaev, U., Orunbaev, S., Negmatullaev, S., 2013. Seismic imaging of subducting continental lower crust beneath the Pamir. Earth Planet. Sci. Lett. 375, 101–112.
Selway, K., Ford, H., Kelemen, P., 2015. The seismic mid-lithosphere discontinuity. Earth Planet. Sci. Lett. 414, 45–57.
Serretti, P., Morelli, A., 2011. Seismic rays and traveltime tomography of strongly heterogeneous mantle structure: application to the Central Mediterranean. Geophys. J. Int. 187 (3), 1708–1724.
Shen, X., Yuan, X., Li, X.Q., 2014. A ubiquitous low-velocity layer at the base of the mantle transition zone. Geophys. Res. Lett. 41 (3), 836–842.
Sodoudi, F., Kind, R., Hatzfeld, D., Priestley, K., Hanka, W., Wylegalla, K., Stavrakakis, G., Vafidis, A., Harjes, H.P., Bohnhoff, M., 2006. Lithospheric structure of the Aegean obtained from P and S receiver functions. J. Geophys. Res. Solid Earth 111.
Sodoudi, F., Yuan, X., Asch, G., Kind, R., 2011. High-resolution image of the geometry and thickness of the subducting Nazca lithosphere beneath northern Chile. J. Geophys. Res. 116.
Sodoudi, F., Yuan, X., Kind, R., Lebedev, S., Adam, J.M.-C., Kästle, E., Tilmann, F., 2013. Seismic evidence for stratification in composition and anisotropic fabric within the thick lithosphere of Kalahari Craton. Geochem. Geophys. Geosyst. 14, 5393–5412.
Sodoudi, F., Brüstle, A., Meier, T., Kind, R., Friederich, W., EGELADOS working group, 2015. Receiver function images of the Hellenic subduction zone and comparison to microseismicity. Solid Earth 6, 135–151.
Soomro, R., Weidle, C., Cristiano, L., Lebedev, S., Meier, T., 2016. Phase velocities of Rayleigh and Love waves in central and northern Europe from automated, broad-band, interstation measurements. Geophys. J. Int. 204 (1), 517–534.
Spakman, W., Wortel, M.J.R., 2004. A tomographic view on Western Mediterranean geodynamics. Chapter 2. In: Cavazza, W., Roure, F.M., Stampfli, G.M., Ziegler, P.A. (Eds.), The Transmed Atlas—The Mediterranean Region From Crust to Mantle. Springer, Berlin, pp. 31–52.
Steer, D.N., Knapp, J.H., Brown, L.D., 1998. Super-deep reflection profiling: exploring the continental mantle lid. Tectonophysics 286 (1–4), 111–121.
Stöckhert, B., Trepmann, C.A., Massonne, H.-J., 2009. Decrepitated UHP fluid inclusions: about diverse phase assemblages and extreme decompression rates (Erzgebirge, Germany). J. Metamorph. Geol. 27, 673–684.
Sumanovac, F., Dudjak, D., 2016. Descending lithosphere slab beneath the Northwest Dinarides from teleseismic tomography. J. Geodyn. 102, 171–184.
Tauzin, B., Debayle, E., Wittlinger, G., 2010. Seismic evidence for global low-velocity layer within the Earth's upper mantle. Nat. Geosci. 3, 718–721.

Tesauro, M., Kaban, M.K., Cloetingh, S., 2008. EuCRUST-07: a new reference model for the European crust. Geophys. Res. Lett. 35, L05313.
Thybo, H., Perchuc, E., 1997. The seismic 8° discontinuity and partial melting in continental mantle. Science 275, 1626–1629.
TOR Working Group, 1999. Important findings expected from Europe's largest seismic array. EOS Trans. 80, 1.
Vecsey, L., Plomerova, J., Babuska, V., PASSEQ Working Group, 2014. Mantle lithosphere transition from the East European Craton to the Variscan Bohemian Massif imaged by shear-wave splitting. Solid Earth 5:779–792. http://dx.doi.org/10.5194/se-5-779-2014.
Villaseñor, A., Ritzwoller, M.H., Levshin, A.L., Barmin, M.P., Engdahl, E.R., Spakman, W., Trampert, J., 2001. Shear velocity structure of central Eurasia from inversion of surface wave velocities. Phys. Earth Planet. Inter. 123, 169–184.
Wessel, P., Smith, W.H.F., 1998. New, improved version of the Generic Mapping Tools released. Eos. Trans. AGU 79, 579.
Wilde-Piorko, M., Geissler, W.H., Plomerova, J., Grad, M., Babuška, V., Brückl, E., Cyziene, J., Czuba, W., England, R., Gaczyński, E., Gazdova, R., Gregersen, S., Guterch, A., Hanka, W., Hegedűs, E., Heuer, B., Jedlička, P., Lazauskiene, J., Keller, G.R., Kind, R., Klinge, K., Kolinsky, P., Komminaho, K., Kozlovskaya, E., Krüger, F., Larsen, T., Majdański, M., Málek, J., Motuza, G., Novotný, O., Pietrasiak, R., Plenefisch, T., Růžek, B., Sliaupa, S., Środa, P., Świeczak, M., Tiira, T., Voss, P., Wiejacz, P., 2008. PASSEQ 2006–2008: passive seismic experiment in Trans-European Suture Zone. Stud. Geophys. Geod. 52, 439–448.
Wilde-Piorko, M., Swieczak, M., Grad, M., Majdanski, M., 2010. Integrated seismic model of the crust and upper mantle of the Trans-European Suture zone between the Precambrian craton and Phanerozoic terranes in Central Europe. Tectonophysics 481, 108–115.
Wortel, M.J.R., Spakman, W., 2000. Subduction and slab detachment in the Mediterranian-Carpathian region. Science 290, 1910–1917.
Yuan, H.Y., Romanowicz, B., 2010. Lithospheric layering in the North American craton. Nature 466, 1063–1071.
Zeh, A., Gerdes, A., 2010. Baltica- and Gondwana-derived sediments in the Mid-German Crystalline Rise (Central Europe): implications for the closure of the Rheic ocean. Gondwana Res. 17, 254–263.
Zhu, H., Tromp, J., 2013. Mapping tectonic deformation in the crust and upper mantle beneath Europe and the North Atlantic. Science 341, 871.
Zhu, H., Bozdag, E., Peter, D., Tromp, J., 2012. Structure of the European upper mantle revealed by adjoint tomography. Nat. Geosci. 5, 493–498.
Zhu, H., Bozdag, E., Tromp, J., 2015. Seismic structure of the European upper mantle based on adjoint tomography. Geophys. J. Int. 201, 18–52.
Zielhuis, A., Nolet, G., 1994. Shear-wave velocity variations in the upper mantle beneath central Europe. Geophys. J. Int. 117, 695–715.